Cerebral Cortex November 2012;22:2587–2601
doi:10.1093/cercor/bhr330
Advance Access publication November 28, 2011

Robo4 Regulates the Radial Migration of Newborn Neurons in Developing Neocortex

Wang Zheng[1,2], An-qi Geng[1], Peng-Fei Li[1,2], Yi Wang[1,2] and Xiao-bing Yuan[1]

[1]Institute of Neuroscience and State Key Laboratory of Neuroscience, Shanghai Institutes for Biological Sciences, Chinese Academy of Sciences, Shanghai 200031, China and [2]Graduate School of the Chinese Academy of Sciences, Shanghai 200031, China

Wang Zheng and An-qi Geng have contributed equally to this work

Address correspondence to Xiao-bing Yuan. Email: yuanxb@ion.ac.cn.

During the morphogenesis of neocortex, newborn neurons undergo radial migration from the ventricular zone toward the surface of the cortical plate to form an "inside-out" lamina structure. The spatiotemporal signals that control this stereotyped radial migration remain elusive. Here, we report that a recently identified Robo family member Robo4 (Magic Roundabout), which was considered to be solely expressed in endothelial cells, is expressed in developing brain and regulates the radial migration of newborn neurons in neocortex. Downregulation of Robo4 expression in cortical newborn neurons by using *in utero* electroporation, with either specific siRNAs in wild-type rodents or with Cre recombinase in floxed-robo4 mutant mice, led to severe defects in the radial migration of newborn neurons with misorientation of these neurons. Moreover, newborn neurons transfected with Robo4 siRNAs exhibited significantly lower motility in a transwell migration assay (Boyden chamber) in the absence of Slit and significantly higher sensitivity to the repulsive effect of Slit in both transwell migration assay and growth cone collapse assay. Overall, our results showed an important role of Robo4 in the regulation of cortical radial migration through Slit-dependent and -independent mechanisms.

Keywords: neocortex, radial migration, repulsion, Robo4, Slit

Introduction

The elaborately regulated migration of newborn neurons is a critical process for the development of brain architecture. Disorders in neuronal migration cause several distinct human syndromes, in which patients often suffer from epilepsy and mental retardation (Bielas et al. 2004; Gressens 2005; Guerrini and Filippi 2005; McManus and Golden 2005). During the development of neocortex, waves of postmitotic neurons exit the ventricular zone (VZ), establish a polarized morphology in the upper subventribular zone (SVZ) and intermediate zone (IZ), and then move in a radial orientation toward the pial surface (Rakic 1990; Hatten 1999; LoTurco and Bai 2006). These newborn neurons take their final positions in the cortical plate (CP) in an "inside-out" sequence, with early-born neurons eventually populating the deeper layers and late-born neurons occupying upper layers (Angevine and Sidman 1961; Berry and Rogers 1965). After neurons have arrived at the appropriate layer, their axons and dendrites extend, branch, and target the correct places to establish functional connections (Rakic and Lombroso 1998; Yu and Bargmann 2001; Colon-Ramos 2009; Feldman 2009).

The spatiotemporal signals that control the stereotyped radial migration remain elusive (Ayala et al. 2007; Marin et al. 2010). It has been reported that neuronal migration and axon pathfinding are guided by extracellular cues including Netrins, Semaphorins, Ephrins, and Slits (Song and Poo 2001; Guan and Rao 2003; O'Donnell et al. 2009). The Slit and Robo family of guidance factors and receptors are repulsive for axon pathfinding and cell migration (Bashaw and Goodman 1999; Brose et al. 1999; Kidd et al. 1999; Li et al. 1999; Nguyen Ba-Charvet et al. 1999; Dickson and Gilestro 2006; Andrews et al. 2007; Guan et al. 2007; Ypsilanti et al. 2010). In vertebrates, 3 *slit* (*slit1-3*) genes and 3 *robo* (*robo1-3*) genes are expressed in the nervous system, and their timely expression is required for pathfinding and branching of axons and the proper migration of neurons and glial cells (Dickson and Gilestro 2006; Andrews et al. 2007; Ypsilanti et al. 2010). Previous studies showed that the repulsive factor Slit1 has abundant expression in CP during cortical development; meanwhile Robo1 and Robo2, receptors that mediate the Slit repulsion, are expressed in cortical neurons (Marillat et al. 2002; Whitford et al. 2002; Andrews et al. 2007). An intriguing question is how these Robo-expressing newborn neurons can invade the Slit1-expressing CP region.

Robo4 is a recently identified Robo family member, which is considered to be an endothelial-specific gene (Huminiecki and Bicknell 2000; Huminiecki et al. 2002). The protein of Robo4 is shorter than other Robos at both intracellular and extracellular domains, with only 2 of the 4 conserved immunoglobin (Ig) and fibronectin (FN) motifs in the extracellular region and 2 of the 4 conserved cytoplasmic motifs (CC0 and CC2) in the intracellular region (Huminiecki et al. 2002). Whether Robo4 could serve as a Slit receptor remains controversial (Verissimo et al. 2009). It has been reported that Robo4 plays important roles in several aspects of vascular development, including the guidance of endothelial cell (EC) migration, regulation of the cell cycle, and inhibition of pathologic angiogenesis and endothelial hyperpermeability (Bedell et al. 2005; Suchting et al. 2005; Kaur et al. 2006; Jones et al. 2008; Kaur et al. 2008; Jones et al. 2009; Sheldon et al. 2009; Chen et al. 2010; London et al. 2010; Marlow et al. 2010; Koch et al. 2011). Although Robo4 was considered to be solely expressed in ECs, there is evidence showing that Robo4 exists in different regions of developing central nervous system (CNS) in zebrafish (Bedell et al. 2005). Interestingly, a recent clinical study showed that a single nucleotide polymorphism (SNP) of Robo4 (rs6590109, $P = 0.009$) is associated with autism in a Caucasian population (Anitha et al. 2008), supporting the notion that Robo4 may play a role in the development and function of human brain. Therefore, the expression of Robo4 and its potential function in developing CNS remain to be clarified.

In the present study, we investigated whether Robo4 could regulate the radial migration of cortical neurons by regulating the guidance signal of Slit. We found that both the mRNA and the protein of Robo4 are expressed in developing brain. Knocking down (KD) of Robo4 expression in newborn cortical neurons by using *in utero* electroporation (IUE) with specific siRNAs in both rats and mice or conditional knockout of Robo4

by IUE with Cre recombinase in floxed-robo4 mutant mice resulted in severe disturbances in the radial migration of newborn neurons, with high chance of misorientation of transfected neurons. In dissociated culture, newborn neurons with reduced Robo4 expression showed significantly reduced motility in transwell migration and enhanced sensitivity to Slit. Together, our findings suggest that the novel Robo family member Robo4 may regulate cortical radial migration, partly through its suppression of Slit repulsion.

Materials and Methods

Animals

All timely pregnant Sprague-Dawley rats and wide type c57 mice used in the present study were provided by SLAC Laboratory Animal Co. Ltd (Shanghai, China). All experimental procedures involving rats and mice were carried out under the guideline and permission of the Animal Care and Administration Committee of the Institute of Neuroscience, Shanghai Institute for Biological Sciences, Chinese Academy of Sciences (NA-100410-5).

Cell Culture

Primary culture of cortical neurons was performed in accordance with previous methods (Zhao et al. 2009). Briefly, cortical tissues from embryonic day 16 (E16) rats were dissected and digested by 0.125% trypsin in phosphate buffered saline (PBS), and dissociated neurons were plated into 35 mm dishes coated with 100 mg mL^{-1} poly-D-lysine. cos-7 cells were plated into 35 mm dishes without coating. In the transfection experiments, neurons or cos-7 cells were transfected with 5 μg of different plasmids by using the Amaxa Nucleofector kit following the protocol provided by the manufacturer. In the Slit-binding experiments, cos-7 cells were transfected with different plasmids. Forty-eight hours after transfection, cells were incubated with 1–15× hSlit2 or control condition medium for 40 min.

Reverse Transcription–Polymerase Chain Reaction and Plasmid Construction

For reverse transcription–polymerase chain reaction (RT-PCR), total RNAs were extracted from rat cortical tissues or cultured cells with Trizol reagent (Invitrogen, Carlsbad, CA) and were converted into complementary deoxyribonucleic acid (cDNA) with a Revert Aid First Strand cDNA Synthesis kit (MBI Fermentas). The forward (FW) and reverse (RW) primers are shown in Table 1. Polymerase chain reaction was carried out using the E18 cortical cDNA with the following protocols: 94 °C, 5 min, 1 cycle; 94 °C, 45 s, 57 °C, 30 s, 72 °C, 90 s, 35 cycles, with a 10 min 72 °C final extension. For *robo1*, there generated a 195 bp DNA band and 130 bp for *robo2*, 228 bp for *robo3*, and 219 bp for *robo4*.

Table 1
Sequences of PCR primers for RT-PCR experiments

Items	Sequence
Robo1RTFW	CACCGAATGCTGCTGCCAAGT
Robo1RTRW	CGCCACCATAACATCTGAAGG
Robo2RTFW	GAGGAGATGGAGGACTAATG
Robo2RTRW	GGCCACTATTGCTGTTGTTG
Robo3RTFW	GTGTGGCTCGCAACTACCTG
Robo3RTRW	CCTCCACGTATGGTGATCCT
Robo4RTFW	AGCTGAGAGCAGCCGTTGACT
Robo4RTRW	CATTCAGCAGCCAGCGGATAG
Robo4FW	ATGGGACAAGGAGAGGAGCTGAG
Robo4RW	CTATGTCCATTCTAAGGGAGGCG
Robo4hFW	ATCGATATGGGCTCTGGAGGAGACAG
Robo4hRW	GTCGACTCAGGAGTAATCTACAGGAG
Robo4F3	GCTTGTGTCCAGGGAAATACG
Robo4R2	TTGGGAAGTCAGCAAATCAGC
RBGlpAdirect1	GTATTTGGTTTAGAGTTTGGC
EmxPCrDirect3	GTGCCATCATGAAGGATGC
Emx3′UTR	GGGGGACATGAGAGGATGTCAC
Robo4ISHFW	CCAGCTGCTAGGCGCCTTCC
Robo4ISHRW	CTGGACAGGTTGCTGGATCCTG

For rat *robo4* cloning, primers were designed according to the sequence of GenBank NM_181375.1. Polymerase chain reaction was carried out using the E18 cortical cDNA with the following protocols: 94 °C, 5 min, 1 cycle; 94 °C, 45 s, 60 °C, 30 s, 72 °C, 90 s, 35 cycles, with a 10 min 72 °C final extension. The PCR products were ligated into pGEM-T vector using T4 ligase (New England Biolab) and sequenced. The result of sequencing is identical to the putative sequence of *robo4* (rat) in GenBank. Robo4-HA was obtained by PCR amplification from pGEM-Robo4 (rat) using primers Robo4FW(KP) and Robo4RW(MF), and the PCR product was inserted into the KpnI/MfeI site of a modified version of p-cDNA 3.1 vector containing a C-terminal fusion of 6 histone (gift from Dr Zuo-ren Wang). Robo4-EGFP was obtained by PCR amplification from pGEM-Robo4 (rat) using primer Robo4FW(MF) and Robo4RW(KP) and ligation of the PCR product into the MfeI/KpnI site of pEGFP-N3. All the primers used are shown in Table 1. Full-length human *robo4* was amplified by PCR using primers Robo4hFW and Robo4hRW from pCMV-Robo4-myc (gift from Dr Jian-guo Geng) and subcloned into the ClaI/XhoI site of pCAG-IRES-EGFP.

Generation of Robo4$^{floxed/floxed}$ Mutant Mice

The targeting strategy for the Robo4 locus is shown in Figure 3*C*. To generate targeting vector, we introduced *loxp* site at both sides of the exon 3 to enable Cre-dependent excision of this exon and generation of a new stop codon. For positive selection of transfected embryonic stem (ES) cells, *neo* expression cassette was placed into intron 2. Additionally, *FRT* sites were placed at both downstream of exon 2 and upstream of the *5′ loxp* sites. These *FRT* sites enabled the excision of the *neo* expression cassette completely by Flp recombinase. After electroporation of the targeting vector into ES cells, G418-resistant clones were collected and correctly targeted clones were identified by Southern blotting and PCR. Chimeric mice were crossed with the C57BL/6 mice to generate F1 mice. Mice carrying the targeted allele were identified by PCR-based genotyping. To remove the *FRT*-flanked *neo* sequence, Robo4$^{neo/neo}$ mice were crossed with mice expressing Flp recombinase ubiquitously to generate Robo4$^{floxed/floxed}$ (termed "floxed-robo4") mice.

Tail DNA was analyzed by PCR using several sets of primers. The *loxp* sites were analyzed with primers Robo4F3 and Robo4R2 amplifying of a 314 bp band and a 212 bp band for wild-type (WT) allele. Sequences of all used primers are shown in Table 1.

In Situ Hybridization

In situ hybridization (ISH) was performed as described previously (Chen, Sima, et al. 2008; Zhao et al. 2009). Briefly, rat cDNA encoding *robo4* was amplified by RT-PCR using cDNA primers Robo4ISHFW and Robo4ISHRW, then subcloned into a pGEM-T vector (Promega). *Slit1* probes are gifts from Dr A. Chedotal (Marillat et al. 2002, 2004). RNA probes were generated by transcription in the presence of the Digoxin-labeled NTP mix (Roche). Brain cryostat sections of 10 μm were hybridized with 1 μg ml^{-1} Digoxin-labeled sense or antisense probes for 16–24 h at 65 °C in hybridization solution (50% formamide, 5× saline-sodium citrate [SSC], 300 μg ml^{-1} yeast tRNA, 100 ng ml^{-1} heparin, 1 mM ethylenediaminetetraacetic acid (EDTA), 1× Denhardt's solution, 0.1% Tween 20, 0.1% 3-[(3-Cholamidopropyl)dimethylammonio]-1-propane-sulfonate, 5 mM EDTA), followed by 2 washes with 2× SSC for 30 min at 65 °C. Then, RNase A (0.5 μg ml^{-1} in 2× SSC) treatment was performed at 37 °C for 30 min. Subsequently, sections were washed twice with 0.2× SSC for 30 min at 65 °C to remove any excess probe and incubated with alkaline phosphatase-labeled anti-Digoxin antibody (1:3000, Roche) at 4 °C overnight. The hybridization signal was visualized with a detection solution (1 μL of Nitrotetrazolium Blue chloride and 3.5 μL of 5-Bromo-4-chloro-3-indolyl phosphate disodium salt in every milliliter of mixture of alkaline phosphatase buffer) in dark at room temperature for 2–12 h.

Immunoblotting and Immunostaining

Western blotting was performed as described previously (Zhao et al. 2009). Briefly, cells were lysed in 0.2 mL of lysis buffer (0.1% sodium

dodecyl sulfate, 1% Nonidet P-40, 50 mM *N*-2-hydroxyethylpiperazine-*N*′-2-ethanesulfonic acid (pH 7.4), 2 mM EDTA, 100 mM NaCl, 5 mM sodium orthovanadate, and 40 M *p*-nitrophenyl phosphate) with 1% Protease Inhibitor Mixture Set I (Calbiochem). To obtain the homogenate of cortical tissue, cortices were first dissected from rats and lysed in 0.1 mL of lysis buffer in tissue homogenizer. Lysates were centrifuged at 12 000 *g* for 25 min. The supernatant was denatured immediately. Anti-Myc (monoclonal, Cell Signaling Technology, 1:1000), anti-GFP (polyclonal, Molecular Probes, 1:1000), and anti-β-actin (monoclonal, Chemicon, 1:3000) antibodies were used.

Brains were removed and fixed in 4% paraformaldehyde after transcardial perfusion. For fluorescence immunostaining, brains were cryopreserved in O.C.T. compound (Sakura). Coronal cryostat sections of 35 μm were cut on a freezing microtome and immediately processed for immunostaining using a 3-step protocol: blocking of nonspecific antigenic sites in 5% bovine serum albumin plus 0.2% Triton X-100, overnight incubation with primary antibodies, and overnight incubation with secondary antibodies. The primary antibodies used were anti-Robo4 (polyclonal, Abcam, 1:200), anti-Tuj1 (monoclonal, Chemicon, 1:1000), anti-Nestin (monoclonal, Chemicon, 1:200), anti-GFAP (polyclonal, DAKO, 1:500), anti-GAD65/67 (polyclonal, Sigma, 1:500), anti-GFP (polyclonal, Molecular Probes, 1:1000; monoclonal, Molecular Probes, 1:200), anti-CD31 (polyclonal, Santa Cruz, 1:200), anti-cleaved caspase-3 (polyclonal, Cell Signaling Technology, 1:200), anti-Ki67 (polyclonal, Novocastra, 1:1000), anti-phospho-Histone H3 (Ser10) (polyclonal, Upstate, 1:200), anti-Pax6 (polyclonal, covance, 1:250), anti-Tbr2 (polyclonal, Abcam, 1:200), and anti-BrdU (monoclonal, Sigma, 1:200). Fluorescently conjugated monoclonal or polyclonal IgG Alexa 488 or Alexa 633 (Molecular Probes, 1:1000) was used as secondary antibodies. Sections were counterstained by 4′,6-diaminodino-2-phenylindole (DAPI; 1:2000) to visualize the nuclei. Images were acquired on a Zeiss LSM 510 multiphoton confocal system using a multitrack configuration, or an Olympus FV1000 confocal microscope, and processed using Image-Pro Plus 6.0/Adobe Photoshop CS. The intensity of fluorescence was measured using the software Image-Pro Plus 6.0. Statistical significance ($P < 0.01$) was assessed using the paired Student's *t*-test.

Preparation of Vector-Based siRNAs

The siRNA sequences were designed using an online design tool (http://www.dharmacon.com) and cloned into a pSuper vector under the control of H1 promoter. The siRNA sequences are given as follow:

Robo4-RNAi1: 5′-ATATGTGTATGGCCACCAA-3′;
Robo4-RNAi2: 5′-GCATTGCTGTGTGTATCTA-3′;
Robo4-RNAiM: 5′-ATATGTGAACGCCCACCAA-3′.

In Utero Electroporation

Plasmids were transfected by using IUE as described previously (Inoue and Krumlauf 2001; Saito and Nakatsuji 2001; Chen, Sima, et al. 2008). Plasmids (3 mg ml^{-1}) were mixed with Fast Green (2 mg ml^{-1}, Sigma) and injected into the lateral ventricle of rat/mice embryos after exposing the uterus. A pair of 10 mm forceps electrode was then placed outside the uterus at the head position. Next, electric pulses were generated by a pulse generator (BTX T830) and applied to the brain: 5 repeats of 60 V for 50 ms with a pulse interval of 100 ms for E16 rats and 5 repeats of 30 V for 50 ms, with an interval of 1 s for E14.5 mice.

Fluorescence-Aided Cell Sorting Purification of Newborn Neurons

Different times after IUE with enhanced yellow fluorescent protein (EYFP), thick coronal sections of cortex were cut with an operating blade by hand, and the CP region or the VZ/SVZ/IZ region of the cortical tissue was dissected with a sharp tungsten needle and collected. Tissues were digested gently with 0.125% trypsin for 10 min at 37 °C, rinsed with PBS, and put on ice. EYFP-labeled cells in the cell suspension were collected by Moflo XDP FASC system (Beckman Coulter). Collected cells were lysed immediately for mRNA extraction.

Time-Lapse Imaging and Collapse Assay

Cortical tissues were transfected with different plasmids by IUE at E16, neurons were dissociated at E18 and seeded on cover glass and cultured for 12 h in Dulbecco's modified Eagle medium plus 10% fetal bovine serum and 2% B27 (Gibico). The culture was transferred to an incubation chamber (37 °C) on the confocal microscope (Olympus, FV1000) with a 40×/0.80 W objective. Time-lapse images were acquired every 5 min. For Slit application, 40× hSlit2CM or 293CM as control was added into the chamber to a final concentration of 1–15×. For the detection and quantification of growth cone (GC) collapsing activities, the protocol followed this reference (Kapfhammer et al. 2007).

Cell Migration Assay

The transwell migration assay was performed as described previously (Zhao et al. 2009). Brains were transfected with different plasmids by IUE at E16, transfected cells were dissociated at E18 and assayed using a Boyden transwell system (5 μm pore size, Corning Costar Co., USA). Before seeding, both sides of the transwell were coated overnight with poly-D-lysine (30 μg ml^{-1}, Sigma). Seven hundred and fifty microliters of serum-free medium (Neurobasal medium, 2% B27, Gibico) containing dissociated cells (5×10^5 cells per well) was added into the upper insert of each chamber. In the bottom chamber, 250 μl of serum-free medium (Neurobasal medium, 2% B27, Gibico) with or without Slit2 (R&D, 6 μg ml^{-1}) was added. The medium was changed 1 day after seeding to maintain the Slit gradient. Two days after seeding, cells were fixed with 4% paraformaldehyde, and cells attached to the upper side of the membrane filter were thoroughly scraped off. Cells attached to the bottom side of the membrane filter were immunostained with the anti-GFP and anti-Tuj1 antibodies by the method described above. Images were taken by using the confocal microscope (Olympus, FV1000).

Morphometry Analysis

For morphometric analysis, at least 4 embryos were analyzed for each condition in parallel experiments, and at least 20 cells were counted from each slice analyzed. The z-series stacks of confocal images were taken from parallel regions of transfected brains by using the confocal microscopes (Zeiss, LSM 510; Olympus, FV1000). The z-series stacks of confocal images were semiautomatically traced using the software Neurolucida and Neuroexplorer. The total length and branch number of each individual process in transfected neurons were analyzed using the program Neuroexplorer. In E18 and P0 transfected cortices (Fig. 2*D*), neurons at IZ with >2 primary processes were counted as multipolar, and the angle between leading process and the neighboring radial glial fiber was measured by using the software Neurolucida and Neuroexplorer (Fig. 4). Statistical significance ($P < 0.01$) was assessed using the Kolmogorov–Smirnov test or Student's *t*-test.

For comparison of neuron distribution, the number of GFP^+ neurons in each subregion (layers II and III, layers IV–VI, IZ-VZ) was counted to calculate the percentages of neurons in each region. Results are shown as mean ± standard error of the mean. Statistical analysis was performed using 1-/2-way analysis of variance (ANOVA) followed by a Bonferroni post hoc test.

For the quantification of the bromodeoxyuridine (BrdU) incorporation rate, E16 embryos were electroporated with various constructs. BrdU was injected at 100 mg kg^{-1} body weight intraperitoneally into pregnant rats 24 h after electroporation. Brains were taken out after another 24 h, and cryostat sections were immunostained with anti-BrdU and anti-Ki67 antibodies. Comparable areas in the neocortex of individual brains were chosen for analysis.

Results

Expression of Robo4 in Developing CNS

To examine whether Robo4 is expressed in rat CNS, RT-PCR, western blotting, and ISH were carried out at different developmental stages. RT-PCR with specific primers showed that from E16 to postnatal day 7 (P7), *robo4* mRNAs were

expressed in the neocortex, hippocampus, and cerebellum (Fig. 1*A*). *Robo4* mRNAs were also detected in the primary culture of E16 cortical neurons (Supplementary Fig. S2*A*). The expression of Robo4 proteins was detected by western blotting in both neocortex and cerebellum (Fig. 1*B*).

Next, we analyzed the expression pattern of *robo4* in developing brain by using ISH and compared it with that of *slit1*. In sagittal sections of P0 rat brain, we observed that *robo4* was widely expressed, with relatively high signal in the olfactory bulb, cerebral cortex, subcortical nuclei, hippocampus, and cerebellum (Fig. 1*D*). In coronal sections of the cerebral cortex, we observed that at E18 *robo4* exhibited wide expression from VZ/SVZ to CP, and *slit1* was expressed in CP. At P0, both *slit1* and *robo4* were expressed in CP, with

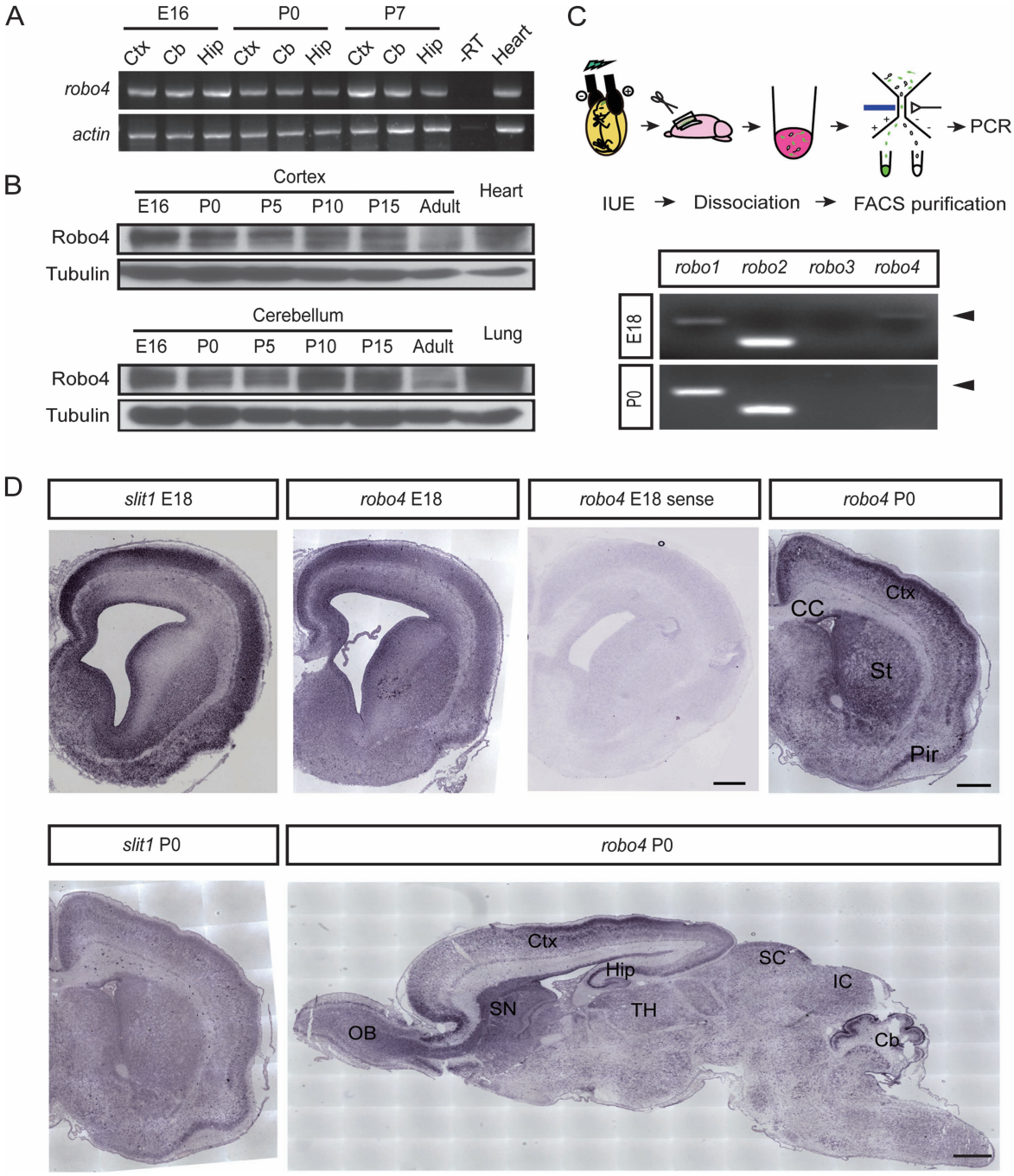

Figure 1. Robo4 is expressed in developing CNS. (*A*) Analysis of *robo4* mRNA expression in rat CNS by RT-PCR. The mRNA from heart tissue was used as a positive control. Rat β-*actin* mRNA was also assayed as a loading control for RT-PCR. "−RT" refers to the PCR reaction performed in the absence of reverse transcriptase. Abbreviation: Ctx, cortex; Cb, cerebellum; Hip, hippocampus. (*B*) Western blotting analysis of Robo4 protein in the cortex and cerebellum. (*C*) Expression of *robo* mRNAs in newborn migrating neurons revealed by semiquantitative RT-PCR at different stages. Embryos were transfected by using IUE at E16. At E18 and P0, EYFP-labeled newborn neurons were dissociated and harvested by FACS. (*D*) ISH using *robo4* and *slit1* riboprobes. In coronal sections of neocortex, *robo4* expression is located in VZ/SVZ and CP from E18 to P0. At P0, *robo4* is expressed in the cortex, subcortical nuclei, hippocampus, midbrain, and cerebellum. Note the partial overlap of *slit1* and *robo4* signal in the somatosensory cortex during development. Scale bar, 500 μm. Abbreviation: OB, olfactory bulb; CC, corpus callosum; SN, striatal neuroepithelium; TH, thalamus; SC, superior colliculus; IC, inferior colliculus; St, striatum; Pir, piriform cortex.

intensive expression of *robo4* at the outmost layer of CP and SVZ (Fig. 1*D*). Semiquantitative RT-PCR was further carried out to examine whether *robo4* and other *robo* family members are expressed in newborn neurons that are undergoing radial migration in neocortex (Fig. 1*C* and Supplementary Fig. S1). After IUE of rat cortex with EYFP at E16 (Inoue and Krumlauf 2001; Saito and Nakatsuji 2001), EYFP-positive newborn neurons were harvested by fluorescence-aided cell sorting (FACS) at E18 and P0, respectively. As shown in Figure 1*C*, *robo1*, *2*, *and 4* were detected in sorted newborn neurons at E18 and P0, whereas another *robo* family member *robo3* was not detected. These above results showed that *robo4* is indeed expressed in developing brain, with expression in a purified population of newborn neurons in cortex.

Disruption of Radial Migration by Knockdown of Robo4

To test whether Robo4 regulates the radial migration of newborn neurons in developing neocortex, we applied IUE to deliver specific siRNAs into cortical progenitor cells and silence the expression of Robo4. Two effective siRNA sequences (Robo4-i1 and -i2) were chosen and cloned into the pSuper vector (Brummelkamp et al. 2002). Point mutations in the most effective siRNA sequence (Robo4-i1) were introduced to decrease its knockdown (KD) efficiency (Reynolds et al. 2004), and the resulting siRNA sequence, Robo4-i1M, was used as a negative control (Supplementary Fig. S2). The KD efficiency of above siRNAs were verified by both semiquantitative RT-PCR in primary culture of cortical neurons and western blotting in culture of HEK293 cells transfected with rat Robo4, respectively (Supplementary Fig. S2). The siRNA constructs were electroporated into cortical progenitors of rat at E16 by using IUE, with cotransfection of a plasmid coding for EYFP to label newborn neurons derived from these progenitors. In cortex transfected with a scramble siRNA (control), EYFP-positive cells were found within the VZ and SVZ 48 h after electroporation. In the subsequent week, most labeled cells migrated out of SVZ, crossed IZ, and reached layers II and III of the CP (Fig. 2*A*). Meanwhile, projecting axons of these labeled layer II and III neurons crossed the midline and invaded contralateral side of the cortex at around P3 (data not shown). Both the developmental sequence and the final morphology of electroporated cells are consistent with previous reports (Rakic 1972; Rakic 1990; Gupta et al. 2002; Marin and Rubenstein 2003; Chen, Sima, et al. 2008), indicating that our gene transfer system is reliable to monitor the normal development process of this group of cortical neurons. We found that most transfected cells in control group (81.80 ± 2.87%) had reached the proper layers (layers II and III) at P5. In contrast, neurons transfected with Robo4-i1 displayed severe retardation in radial migration (Fig. 2*B*–*C*), with about 78% of total cells unable to reach layers II and III. Most ectopic cells (71.84 ± 3.52%) failed to enter the CP and stayed below the white matter (WM). Another effective siRNA of Robo4 (Robo4-i2) also markedly suppressed the radial migration of transfected neurons, whereas the mutated siRNA (Robo4-i1M) had no such effect (Fig. 2*B*–*C*). Overexpression of the RNAi-resistant human Robo4 homologue (hRobo4) along with Robo4-i1 prevented above migration defects, with most transfected neurons (79.74 ± 4.42%) migrated to the appropriate layer (Fig. 2*B*–*C*), indicating that the observed migration retardation was caused by specific loss-of-function of Robo4. Moreover, at P20, ectopic neurons could still be observed in deep layers (layers IV–VI and WM) of Robo4-i1-treated brains (Supplementary Fig. S7), suggesting that Robo4-KD led to a permanent defect of neuronal migration. We noted that at E18, 48 h after IUE, we did not observe significant difference in the distribution of transfected cells in different layers of cortical tissue (CP/IZ/SVZ/VZ) in control and Robo4-i1-treated brains (Supplementary Fig. 3*E*), suggesting that Robo4-KD may not cause the arrest of the polarization process of newborn neurons in SVZ/IZ and may not affect the early stage migration of these newborn neurons from VZ/SVZ to IZ. Furthermore, in the SVZ/IZ region of E18-P0 rat cortex, where newborn neurons undergo transition from multipolar to monopolar/bipolar morphology, we did not observe significant differences in the percentages of multipolar and monopolar/bipolar neurons between control and Robo4-i1-treated group, neither the length of the leading process of monopolar/bipolar neurons (Fig. 2*D*). Thus, Robo4 may not be required for the polarization of newborn cortical neurons during early development.

The above results suggest that Robo4 contributes to the proper radial migration of layer II and III cortical neurons. Similar migration retardation was observed in mice after IUE (from E14.5 to E18.5) with Robo4-i1 (same target sequence in mouse), which caused more than half of transfect cells fail to enter the CP (Robo4-i1: 55.69 ± 5.67% vs. control: 15.79 ± 3.54%, Fig. 3*A*). Further studies were carried out in *robo4* conditional knockout mice. We generated a floxed-robo4 mutant line of mouse, in which the *robo4* gene could be deleted by Cre-mediated recombination (see Materials and Methods). Mice with homozygote floxed-robo4 alleles appeared healthy with no obvious differences in their growth and fertility compared with their WT and heterozygous littermates. Knockout of *robo4* in the forebrain by crossing the floxed-robo4 mutant with the Emx1Cre line (Emx1Cre, Robo4$^{floxed/floxed}$) did not result in gross abnormality in the cortical lamination, as shown by the normal distribution pattern of Cux1-possitive neurons in upper layers of cortex and Foxp2-possitive neurons in deeper layers (Supplementary Fig. S8*A*–*C*). However, acute deletion of *robo4* in a small population of newborn neurons by IUE with a plasmid encoding the Cre recombinase into the cortex of floxed-robo4 mutant mice (E14.5–E18.5) resulted in a severe retardation of the radial migration of transfected neurons (Fig. 3*C*). In contrast, IUE of Cre recombinase in WT littermates or IUE of control vector (GFP) in homozygote floxed-robo4 littermates did not affect the radial migration of transfected cortical neurons. Furthermore, IUE of Robo4-i1 caused migration retardation of transfected neurons in WT littermates (Emx1Cre, Robo4$^{+/+}$) but did not affect the radial migration of transfected neurons in homozygote knockout littermates (Emx1Cre, Robo4$^{floxed/floxed}$, Supplementary Fig. S8*D*,*E*), suggesting that the migration retardation after IUE of Robo4-i1 was indeed caused by the acute loss-of-function of Robo4, and Robo4 regulates the radial migration of newborn neurons during cortical development.

Misorientation of Robo4-KD Neurons

Interestingly, neurons at the border between IZ and CP in P0 cortex exhibited a high chance of misorientation after Robo4-KD. As shown in Figure 4, both the average angle between the leading process and the neighboring radial glial fiber and the percentage of abnormal orientated neurons (the absolute angle > 15°) (Hashimoto-Torii et al. 2008) in Robo4-KD group were

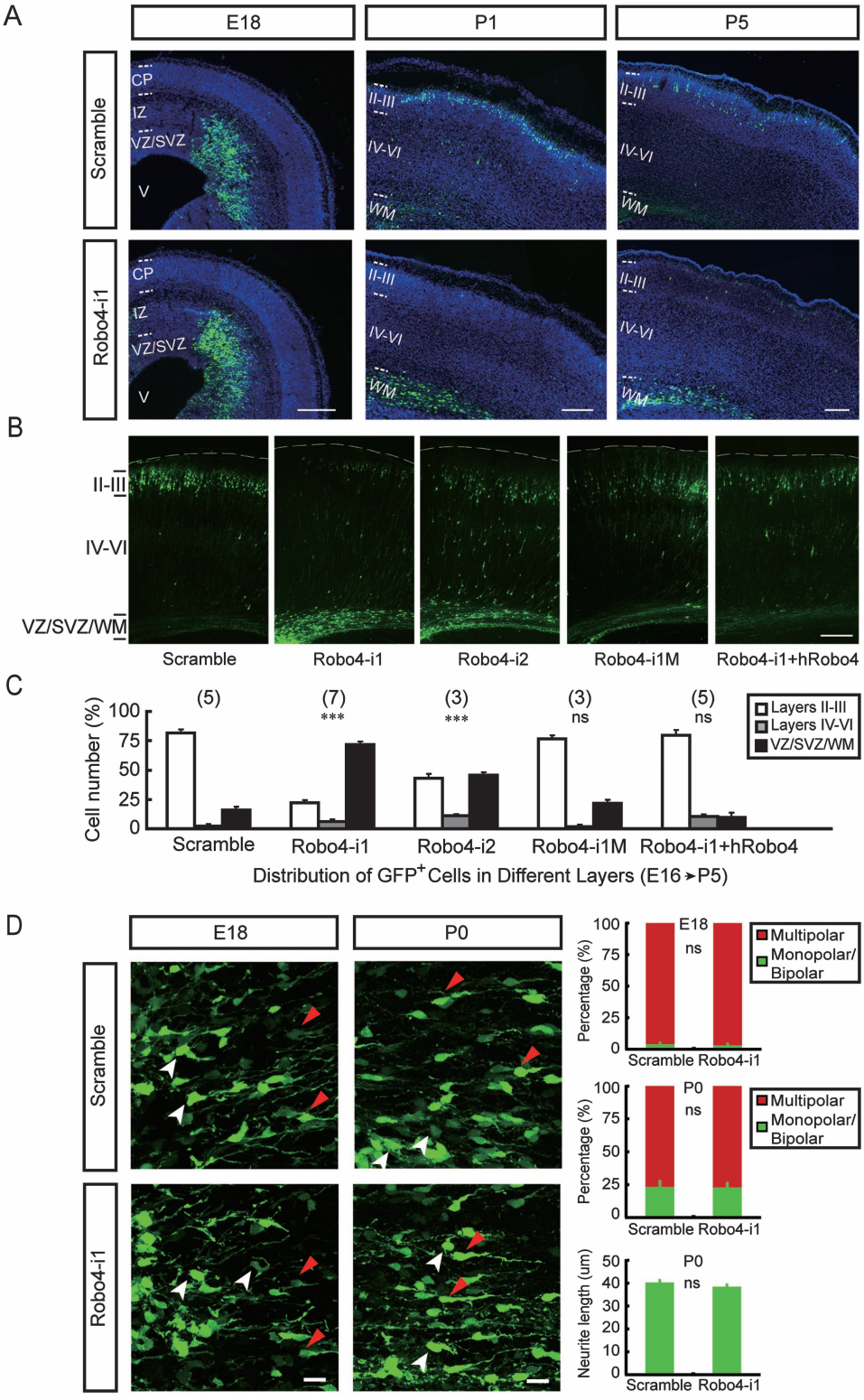

Figure 2. Retardation of cortical radial migration in rats by Robo4 downregulation. (*A*) Representative images of coronal sections of rat somatosensory cortex at different days after IUE of scramble or Robo4 siRNA constructs (E16–P5). Sections were immunostained for GFP (green) and counterstained with DAPI (blue). Scale bar, 250 μm. (*B*) Representative images of coronal sections of P5 rat somatosensory cortex transfected at E16 with different siRNA constructs using IUE including 2 effective siRNA sequences against *robo4* (Robo4-i1 and -i2), a 3-point mutation sequence of Robo4-i1 (Robo4-i1M), and Robo4 siRNA mixed with human Robo4 homologue (Robo4-i1 + hRobo4, rescue). (*C*) Histograms showing the percentages of transfected cells at different regions of P5 rat cortex (mean ± standard error of the mean, $^{***}P < 0.001$). Numbers in brackets are numbers of brains analyzed in each group. Scale bar, 200 μm. (*D*) Knockdown of Robo4 did not affect the polarization of transfected cells. Representative images of transfected neurons in the SVZ and IZ of control or Robo4-i1-transfected cortical sections are shown in the left. Quantification of the proportion of monopolar/bipolar (red arrow) and multipolar (white arrow) GFP^+ neurons and average length of leading neurites are shown in the histograms. Cells exhibiting more than 2 primary processes were counted as multipolar. For each condition, 4 sections (1 section per embryo) with at least 20 cells from each section were analyzed in parallel experiments (mean ± standard error of the mean). Scale bar, 20 μm.

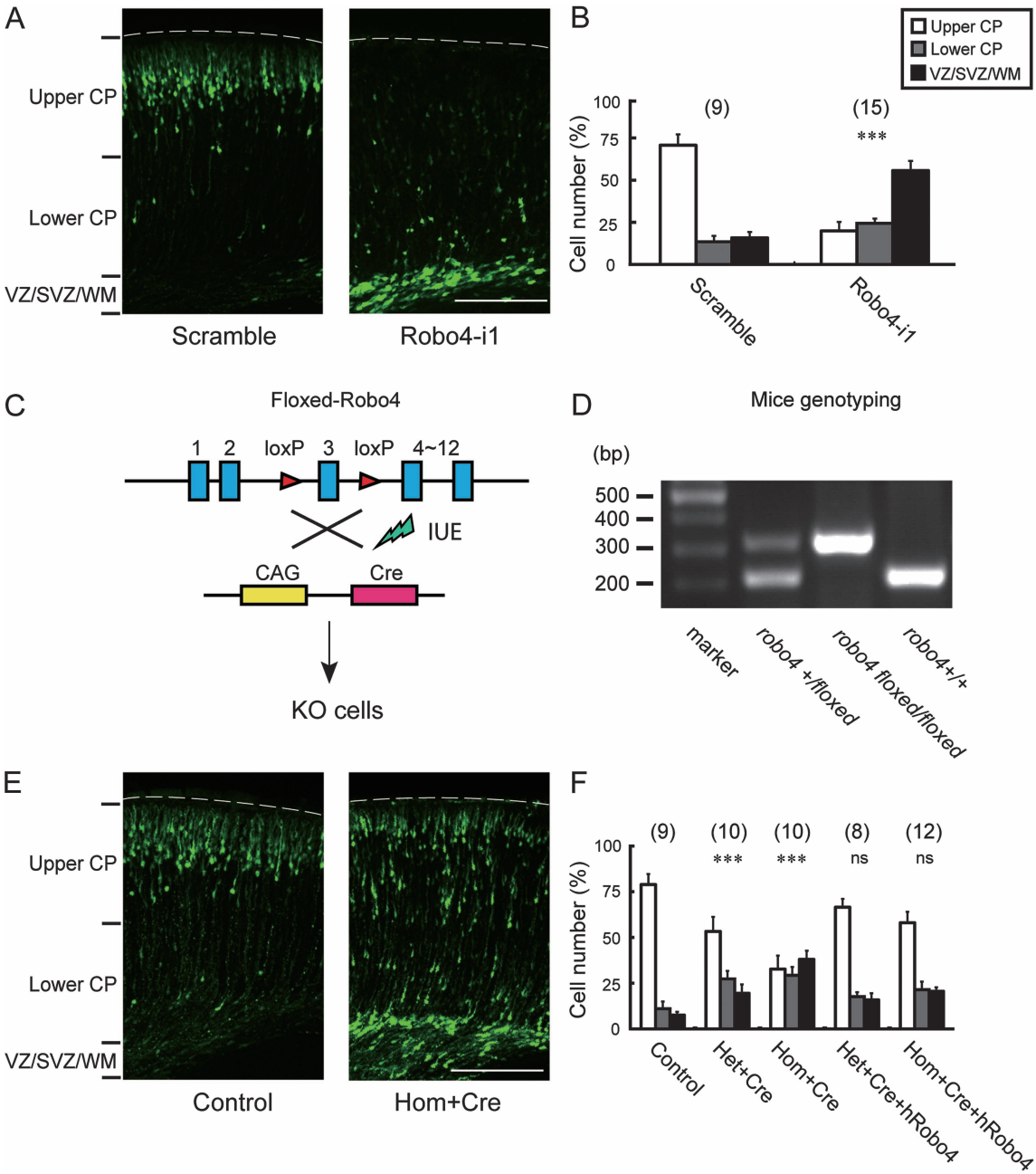

Figure 3. Retardation of cortical radial migration in mice by Robo4 downregulation. (*A*) Representative images of coronal sections of somatosensory cortices from E18.5 mice transfected at E14.5 with EYFP and different siRNA constructs using IUE (scramble siRNA, Robo4-i1). (*B*) Quantification of neurons in different layers (upper CP, lower CP, and VZ/SVZ/WM) of cortex at E18.5. Data are mean ± standard error of the mean (***$P < 0.001$). Numbers in brackets are numbers of brains analyzed in each group. Scale bar, 200 μm. (*C*) Schematics of *robo4* knockout in mice. The third exon of *robo4* gene was flanked by the *loxp* recombination sequence (see Materials and Methods). Knockout of *robo4* in newborn neurons was carried out by IUE with Cre recombinase in floxed-robo4 mice at E14.5. (*D*) PCR analysis of genomic DNA from Robo4$^{+/+}$, $^{+/floxed}$, and $^{floxed/floxed}$ animals. The DNA band for WT allele is 212 and 314 bp for the floxed allele. (*E*) Representative images of coronal sections of E18.5 brains of floxed-robo4 mice IUE with control vector or Cre recombinase. Scale bar, 200 μm. (*F*) Quantification of neurons in different layers of cortex at E18.5 (mean ± standard error of the mean, ***$P < 0.001$).

significantly higher than those in control group. At P20, many ectopic neurons in Robo4-i1-treated cortex exhibited simplified morphology and reversed orientation (Supplementary Fig. S7). This abnormal orientation of migrating neurons in P0 brains and of ectopic neurons in P20 brains is consistent with a gain of repulsion from the CP after Robo4-KD.

Cell-Autonomous Role of Robo4 in Newborn Neurons

The proper radial migration of newborn neurons is known to depend on the radial scaffold. However, by immunostainning of E18 rat brain slices with the anti-Nestin antibody, we found no obvious morphological changes of the radial glial scaffold after transfection with Robo4-i1 (data not shown).

After immunostaining with the antibody against the specific vascular cell marker CD31, we found no GFP-positive vascular cells in transfected brain slices. Thus, although Robo4 may be expressed in vascular cells (Huminiecki et al. 2002; Jones et al. 2008), our IUE could only transfect neural progenitors lining the ventricle wall but not vascular cells within the brain tissue. Moreover, the distribution and density of vascular cells in

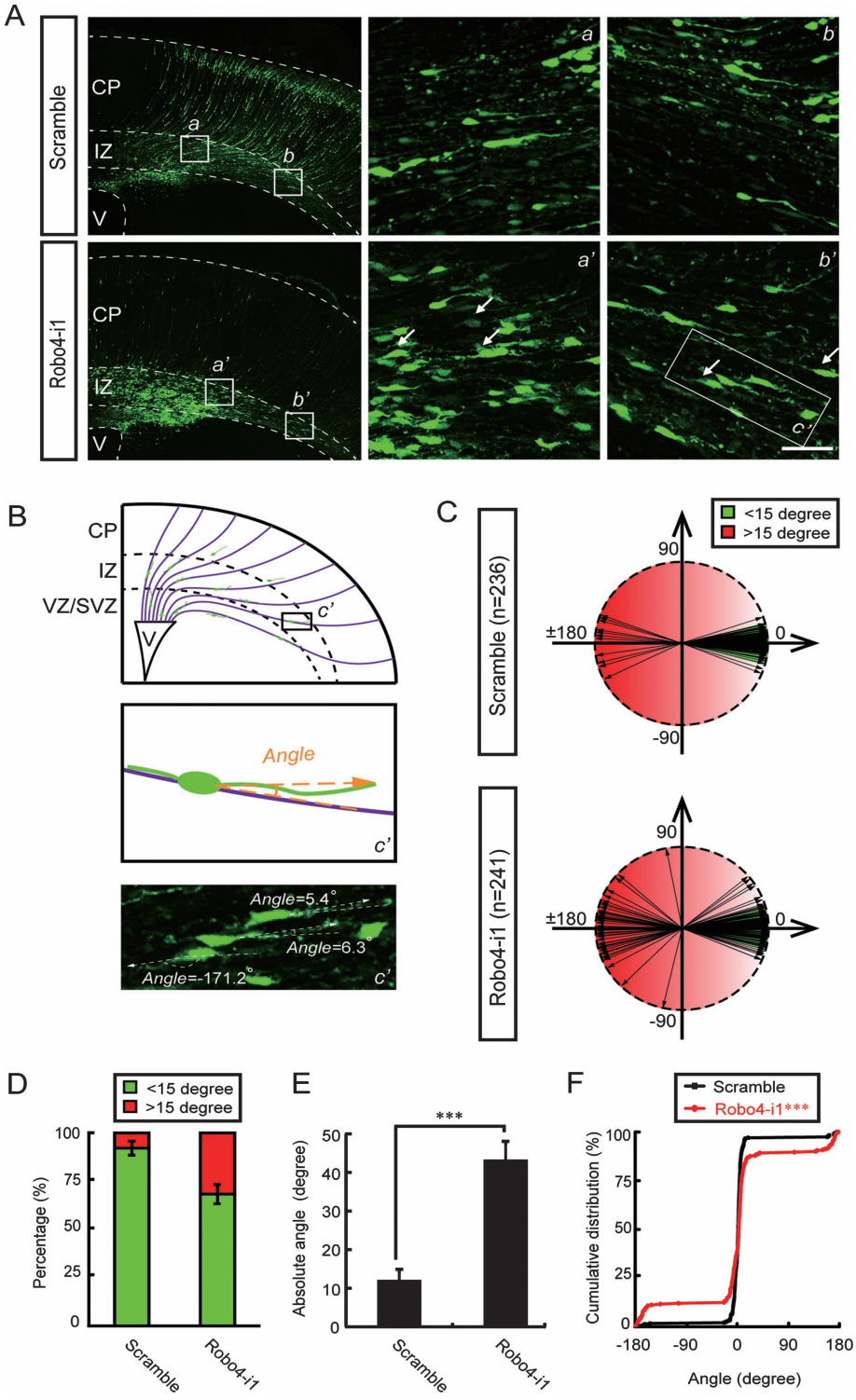

Figure 4. Misorientation of leading processes of migrating neurons by Robo4 downregulation. (*A*) Representative images of migrating neurons from P0 cortices electroporated at E16 with control or Robo4-i1 siRNAs. The selected regions in the left panels are shown in high magnification at right (*a*,*b*; *a′*,*b′*) and the selected region in the right panel *b′* (*c′*) was shown in high magnification below in (*B*). The dash lines indicate the pial surface of brain slices and boundaries of different layers, and white arrows show neurons with reversed leading processes. Scale bar, 25 μm. (*B*) Schematic cartoon showing the measurement of the angle between the leading process and neighboring radial glial fiber. The selected regions (*c′*) in (*A*,*b′*) are shown in high magnification as the paradigm. Arrow indicated the direction from cell body to the tips of leading process and minus angle indicated the leading process of the neuron was beneath neighboring radial glial fiber. (*C*) Polar plot showing the distributions of angles between the leading processes of transfected neurons and the neighboring radial glial fibers as indicated in (*B*). Cells located at the border between IZ and CP with bipolar migratory morphology were analyzed. The angles within ±15° were defined as "oriented normally" (green) (Hashimoto-Torii et al. 2008). Results are from at least 4 cortical sections in each group. (*D*) The percentages of normal orientated and abnormal orientated neurons in control and Robo4-i1-electroporated rat cortices (mean ± standard error of the mean, $^{**}P < 0.01$). (*E*) The histogram showing the averaged absolute angles between leading progress and neighboring radial glial fiber in control and Robo4-i1-electroporated rat cortices (mean ± standard error of the mean, $^{***}P < 0.001$). (*F*) The cumulative percentage plot showing the distribution of the angle between the leading progress and the neighboring radial glial fiber in control and Robo4-i1-electroporated rat cortices described in (*C*) ($^{***}P < 0.001$, Kolmogorov–Smirnov test).

transfected brain regions, as revealed by anti-CD31 staining (Marteau et al. 2011), appeared not affected after IUE of Robo4 siRNA in the cortex. Thus, the radial migration defect after Robo4-KD was not due to the perturbation of the vascular development (Supplementary Fig. S6).

Previous studies suggested that soluble extracellular domain of Robo4 may cause cell cycle arrest at the G1/S phase and inhibit the proliferation of human umbilical vein ECs (HUVEC) (Suchting et al. 2005). To investigate whether Robo4-KD in cortical progenitors influences their proliferation, we analyzed the BrdU incorporation rate and the percentage of cells expressing the mitotic cell marker Ki67 (Supplementary Fig. S3). We defined a BrdU index as the percentage of BrdU– and GFP double–positive cells ($BrdU^+/GFP^+$) in total transfected cells (GFP^+) and a cell-cycle-exit index as the ratio of $GFP^+/BrdU^+/Ki67^-$ cells to $GFP^+/BrdU^+$ cells (Sanada and Tsai 2005; Xue and Yuan 2010). We found no significant difference in either BrdU index or cell-cycle-exit index between control group (scramble siRNA, 16.13 ± 1.70% and 32.87 ± 4.31%, respectively) and the Robo4-KD group (22.06 ± 2.74% and 38.53 ± 3.28%, respectively) (Supplementary Fig. S3*A*,*B*). These results suggest that the proliferation of cortical progenitor cells was not affected after Robo4-KD, and the defective neuronal positioning triggered by Robo4-KD does not seem to be the secondary effect of altered proliferation of transfected progenitor cells.

We next examined the fate of cells derived from transfected progenitor cells by immunostainning using specific markers for various cell types, including Pax6 for progenitors in VZ, Tbr2 for intermediate progenitors in SVZ, GFAP for astrocytes, Nestin for radial glial cells, and GAD65/67 for interneurons (Supplementary Figs S3 and S4). In E18 rat cortices, no obvious difference was found in the percentages of $Tbr2^+/GFP^+$ or $Pax6^+/GFP^+$ cells between control and Robo4-i1-treated groups (Supplementary Fig. S3*C*–*D*). In P5 brain slices, we found that transfected cells located at layers II and III developed the typical morphology of projecting neurons in both control and Robo4-KD groups. In Robo4-KD brain, ectopic cells located at the WM and SVZ were negative for GFAP, Nestin, and GAD65/67 (Supplementary Fig. S4). Therefore, these ectopic neurons in the Robo4-KD brain had adopted the proper pyramidal neuronal fate without differentiating into astrocytes or interneurons. In addition, by comparing the immunostaining signal of the cleaved caspase-3 (the active form of caspase-3), we found no obvious increase in the apoptosis of transfected cells after Robo4-KD, as revealed by similar ratio of cleaved caspase-3–positive cells in the transfected side and the untransfected side of the same cortical section with or without Robo4-KD (Supplementary Fig. S5).

Taken together, these above results suggest that Robo4 plays a cell-autonomous role in the radial migration of newborn neurons, with no significant effect on the proliferation or fate commitment of neural progenitor cells or the development of the radial scaffold.

Potential Mechanism Underlying the Promigratory Function of Robo4

How does Robo4 contribute to the cortical radial migration? As a Robo family member, whether Robo4 could interact with Slit proteins and mediate Slit repulsion remains controversial (Verissimo et al. 2009). To determine whether Robo4 could function as a Slit receptor in migrating neurons, we first investigated the ability of Robo4 to bind Slit using a cell surface binding assay in COS-7 cells. Full-length rat Robo4 tagged with GFP (rRobo4-GFP) and human Robo4 tagged with flag epitope (hRobo4-flag) were transfected into cos-7 cells, with parallel transfection of human Robo2 tagged with GFP (hRobo2-GFP) into COS-7 cells as positive control. Forty-eight hours after transfection, cells were incubated with human Slit2-myc conditioned medium (hSlit2CM) for 40 min (Brose et al. 1999; Li et al. 1999). After carefully washing out the excessive conditioned medium, the expression of Robos and surface-bound Slit were examined by western blotting and immunocytochemistry using antibodies against above epitopes. We found that Robo2, but not Robo4, could bind Slit2 protein on the cell surface (Supplementary Fig. S9). Therefore, our data, together with previous reports, support the notion that the affinity between Robo4 and Slit protein is extremely low comparing with Robo2 (Suchting et al. 2005; Koch et al. 2011) and that Robo4 is unlikely to directly mediate the Slit signaling as a Slit-binding receptor.

Previous studies showed that another Robo family member Robo3, which does not bind with Slit (Camurri et al. 2005; Mambetisaeva et al. 2005), could silence the Slit repulsion mediated by Robo1 and Robo2 in commissural axons in both spinal cord and hindbrain (Marillat et al. 2004; Sabatier et al. 2004; Camurri et al. 2005; Chen, Gore, et al. 2008). To test whether Robo4 could also suppress Slit repulsion in cortical neurons, we further examined the Slit responsiveness of newborn neurons in the presence or absence of Robo4 in dissociated culture of newborn neurons. Brains were transfected with Robo4-i1 or control vector by IUE at E16 as described above, and EYFP-positive newborn neurons were dissociated at E18 and cultured for 12 h (Fig. 5). The application of hSlit2CM (1–15×, Fig. 5*C*) did not cause remarkable morphological changes within 40 min in control neurons (transfected with scramble siRNA), with most (>65%) of the GCs remained intact (Fig. 5*Ba*,*a*′). However, in Robo4-KD neurons, same treatments triggered significantly higher percentages of collapsed GCs in a dosage-dependent manner (Fig. 5*Bb*,*b*′), suggesting that Robo4-KD neurons gained the sensitivity to hSlit2CM. In further time-lapse imaging experiments, dramatic collapse of GCs and shrinkage of neurites were observed in Robo4-KD neurons but not in control neurons in response to hSlit2CM application (Fig. 5*D*). Together, these results showed that Slit is a potential collapsing factor to these newborn cortical neurons only when Robo4 was downregulated and that Robo4 expression may protect migratory neurons from Slit repulsion coming from the CP.

Robo4 Regulates Neuronal Migration through Both Slit-dependent and -independent mechanisms

Robo4 signaling has been implicated in EC migration during angiogenesis both *in vitro* and *in vivo* (Legg et al. 2008; Weitzman et al. 2008). To further study how Robo4 promotes neuronal migration, the transwell migration assay (Boyden chamber assay) was performed in newborn neurons with or without Robo4-KD. As previously reported (Chen, Sima, et al. 2008; Zhao et al. 2009), newborn neurons were first transfected with EYFP along with plasmids coding for siRNAs by IUE at E16, and at E18 EYFP-positive neurons were obtained from IZ of cortex and plated into the Boyden chamber and cultured for 48 h (Fig. 6). We found that the number of transfected neurons migrated to the lower chamber were markedly

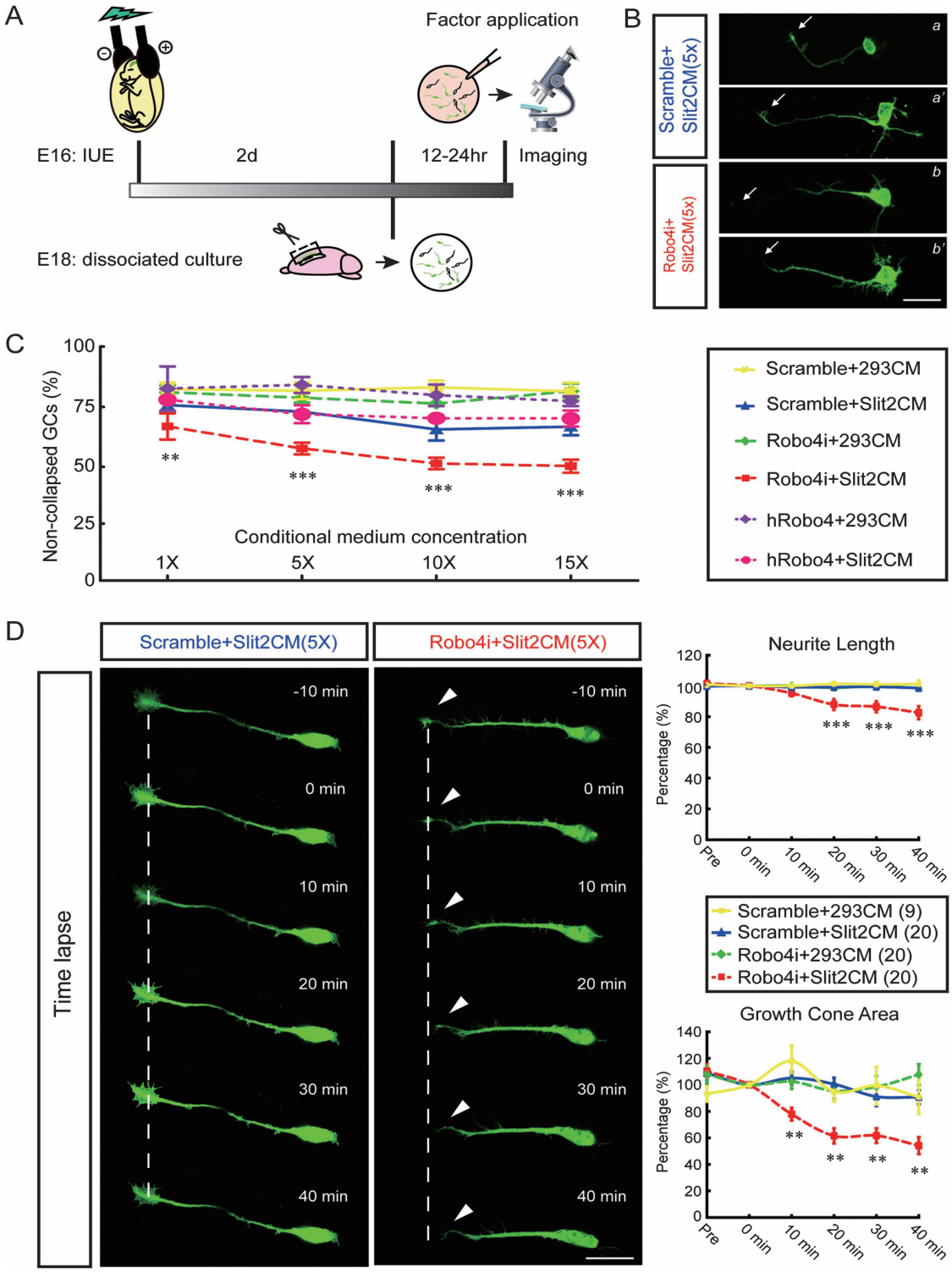

Figure 5. GC collapse triggered by Slit upon Robo4 downregulation. (*A*) Schematic diagram of the GC collapse assay. Neurons transfected by IUE were dissociated from the IZ 2 days after IUE and cultured for 12–24 h. Before observation, hSlit2 conditional medium (hSlit2CM) or control medium (conditional medium from culture of 293 cell line, 293CM) was applied into the bath of neuronal culture. (*B*) Fluorescence images of fixed cortical neurons after 40 min treatment of Slit or control CM. Two typical control cells (transfected with scramble siRNA, upper) and Robo4-KD cells (transfected with Robo4-i1, below) with Slit2CM treatment are shown. Arrows indicate the collapsed GCs. (*C*) Line curves showing the percentages of neurons with noncollapsed GCs at the tip of the longest neurite in response to increasing concentrations of different CMs. Neurons were transfected with scramble or Robo4-i1 siRNA or hRobo4 as indicated in (*A*). Data are from at least 3 independent experiments (mean ± standard error of the mean, $^{**}P < 0.01$, $^{***}P < 0.001$). (*D*) Time-lapse imaging of transfected neurons at various times (number in minute) before and after application of Slit2CM or 293CM. Cells were transfected and cultured as above. A control cell (transfected with scramble siRNA, left) and a Robo4-KD cell (transfected with Robo4-i1, left) incubated with Slit2CM are shown as examples. The dash lines indicate the centers of GCs at −10 min, and the arrow indicates the collapsing GC. Scale bar, 20 μm. Quantifications of normalized changes in neurite length and GC area after application of different CM are shown in the graphs at right. Numbers in brackets are numbers of cells analyzed in each group. Data from each time points (mean ± standard error of the mean) have been normalized to the value at start time (0 min) ($^{**}P < 0.01$, $^{***}P < 0.001$).

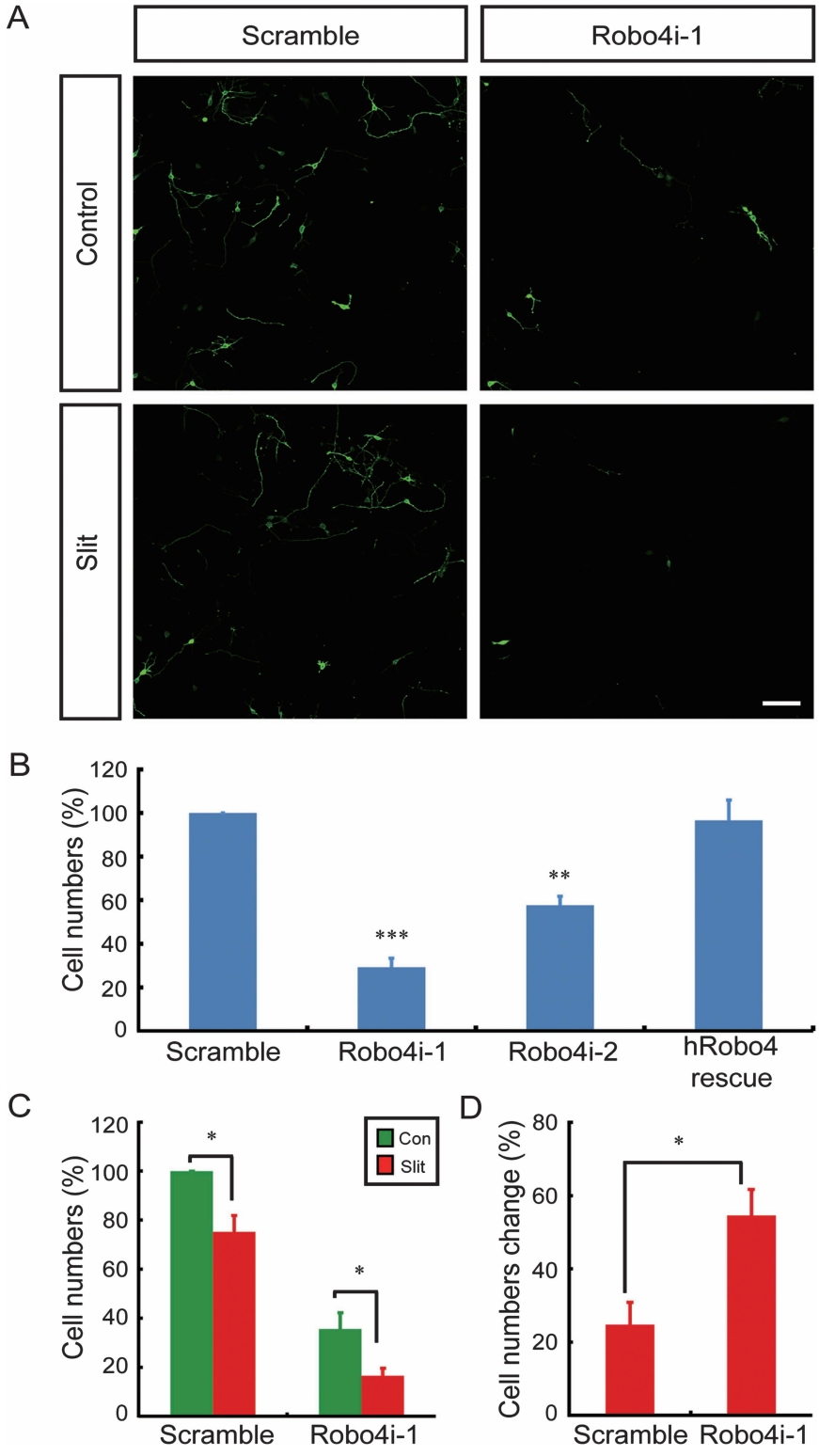

Figure 6. Decrease of neuron motility and increase of Slit sensitivity upon Robo4 knockdown. (*A*) Representative images of newborn cortical neurons transfected with different constructs on the bottom side of the chamber. Two days after seeding, cells were fixed and immunostained with anti-GFP and anti-Tuj1 (not shown here) antibodies. Scale bar, 50 μm. (*B*) Histogram showing the average numbers of transfected neurons that had migrated to the bottom chamber in serum-free medium. Numbers of migrated neurons were normalized to the value of the parallel control. hRobo4 rescue, cotransfection of Robo4-i1 and hRobo4. (*C*) Histogram showing the average numbers of transfected neurons that had migrated to the bottom chamber in the absence or presence of Slit2 (6 μg ml^{-1}) in the bottom chamber. (*D*) Histogram showing the significant higher percentage of reduction of transwell migration in response to Slit2 in Robo4-i1-transfected neurons compared with control neurons (scramble). Data are mean ± standard error of the mean, $^{*}P < 0.05$, $^{**}P < 0.01$, $^{***}P < 0.001$.

decreased upon Robo4-KD (Robo4-i1, 29.21 ± 3.71%; Robo4-i2, 33.35 ± 12.01%, respectively), an effect that could be restored by cotransfection with hRobo4 (Fig. 6*B*). These results suggest that Robo4 is required for the basal motility of these young neurons. To test whether Robo4 regulates the guidance signal of Slit, we added recombinant mouse Slit2 (6 μg ml^{-1}) to the lower chamber. We found that transwell migration of young neurons was suppressed by Slit2 in neurons transfected with scramble siRNA (a 24.76 ± 6.10% reduction comparing with untreated control), suggesting a repulsive effect of Slit to these young neurons (Fig. 6*C,D*). Interestingly, the repulsive effect of Slit was dramatically enhanced by Robo4-KD (a 54.56 ± 6.55% reduction of transwell migration comparing with untreated control, Fig. 6*C,D*). These data suggest that Robo4 expression in newborn neurons may suppress the responsiveness of these young neurons to the repulsive factor Slit and that Robo4 may regulate neuronal migration through both Slit-dependent and -independent mechanisms.

Discussion

Robo4 Expression in Brain

It was reported that Robo4 expression was restricted in vascular system, and its expression was undetectable in the early CNS (before E10) and adult brain of rodent (Fujiwara et al. 2006). However, there were a few studies concerning its expression in developing brain, and only one article reported persistent *robo4* expression in several CNS regions of zebrafish, including the telencephalon, hindbrain, and spinal neural tube (Bedell et al. 2005). In the present study, expression of Robo4 in developing CNS was revealed by RT-PCR, western blotting, and ISH. Robo4 mRNA could be detected in different regions including the neocortex, cerebellum, and hippocampus (Fig. 1*D*). Moreover, its expression was identified by RT-PCR in a purified population of migrating neurons in cortex (Fig. 1*C*). Comparing with previous studies, our work mainly focused on the middle to late embryonic stages of brain, which were not examined by other researchers. Together with the aberrant neuronal migration that we observed upon Robo4-KD, our results suggest that Robo4 is indeed expressed in CNS.

Robo4 Regulates Cortical Radial Migration

We found that downregulation of Robo4 by IUE of specific siRNAs suppressed the radial migration of newborn cortical neurons. No obvious lamination defect was observed in the cortex of Robo4 conditional knockout mice (Supplementary Fig. S8). This may due to the compensation of Robo4 function by other unknown molecules that play redundant functions during development. However, acute knockout of Robo4 by IUE of Cre into a small group of newborn neurons suppressed their migration (Figs 2 and 3). Moreover, IUE of specific Robo4 siRNA led to migration retardation in WT mice (Emx1Cre, $Robo4^{+/+}$) but not in homozygote knockout littermates (Emx1Cre, $Robo4^{floxed/floxed}$) (Supplementary Fig. S8*D,E*), further supporting the notion that migration retardation after IUE of Robo siRNA was indeed caused by downregulation of Robo4 but not by any potential off-target effect of siRNA.

At an early stagy after IUE of Robo4 siRNA (E18), we did not observe significant changes in the distribution of transfected neurons in different cortical layers (Supplementary Fig. 3*E*), suggesting that Robo4 may not play regulatory roles in the polarization process of newborn neurons or their early stage migration. Consistent with this notion, we found no significant difference in the percentage of polarized neurons at SVZ and IZ region between control and Robo4-KD brain (Fig. 2*D*). Moreover, no significant effect was found on the proliferation or differentiation of neural progenitor cells after Robo4-KD (Supplementary Figs S3 and S4). Taken together, these results suggest that Robo4 in newborn cortical neurons mainly contribute to their proper radial migration from IZ to CP.

No defects were observed in the morphology of radial glial scaffold after IUE of Robo4 siRNA, and the vascular cells could not be transfected under our IUE protocol (Supplementary Fig. S6). Moreover, both the Slit responsiveness of GCs and the transwell migration of neurons were affected in dissociated culture of cortical neurons transfected with Robo4 siRNA (Figs 5 and 6). Thus, Robo4 may play a cell-autonomous role in the radial migration of newborn neurons. Yet, cell-nonautonomous role of Robo4 in cortical radial migration could not be ruled out.

Slit-Dependent and -Independent Function of Robo4

Slit/Robo signaling as axon guidance factor/receptor has been extensively studied in the developing nervous system. However, whether Robo4 is a potential Slit receptor remains a heat debate. Direct interactions between Slit and Robo4 have been shown by coimmunoprecipitation assays (Park et al. 2003), but this interaction could not be detected in purified recombinant proteins by Biacore assays (Suchting et al. 2005). Detailed structure–function studies have shown that the second leucine-rich repeats domain of Slit that binds to the first 2 Ig domains of Robo family members (Morlot et al. 2007). Since the extracellular domain of Robo4 lacks the first 2 conserved Ig domains, there should be no or very weak molecular interaction between Slit and Robo4 proteins (Morlot et al. 2007; Hohenester 2008). Our current results further support this notion since we did not observe clear binding of hSlit2 proteins to the surface of cells expressing either human or rat Robo4 (Supplementary Fig. S9).

Despite the lack of direct interaction between Slit and Robo4, our present results, together with previous reports (Kaur et al. 2008; Marlow et al. 2010), showed a clear signaling cross talk between Slit and Robo4. It has been shown that the regulation of Slit/Robo4 signaling plays important roles in the guidance of EC migration and the inhibition of pathologic angiogenesis and vascular hyperpermeability (Legg et al. 2008; Weitzman et al. 2008; Liao et al. 2010). Emerging evidence suggests that a coreceptor is required for Robo4 activation by Slit. For example, Robo1 has been shown to coexist and interact with Robo4 in ECs and coordinate with Robo4 to guide the migration of these cells (Kaur et al. 2008; Sheldon et al. 2009; Marlow et al. 2010). Similar mechanisms may be used in the regulation of cortical neuronal migration.

Our results provide the first evidences that Robo4 plays an important role in CNS development, partially by regulating Slit signaling. First, we found that the mRNAs of *slit1* and *robo4* exhibit overlapping expression regions during cortical development (Fig. 1*D*), suggesting that Robo4 may regulate the Slit responsiveness of cortical newborn neurons. Second, we observed misorientation of neurons after knockdown of Robo4 in developing rat cortex, potentially caused by repulsion of CP-derived Slit1 (Fig. 4 and Supplementary Fig. S7). This notion was further supported by results from the *in vitro* GC collapse

assay and transwell migration assay. An intriguing future question is to examine whether Robo4 exerts its function by directly interacting with other Robo family members (Robo1/2) in these migratory neurons.

Recent reports suggest that Robo4 overexpression in ECs can trigger diverse signaling cascades, some of which are considered as ligand independent. For example, transfection of full-length Robo4 alone into HUVECs induced filopodia formation (Sheldon et al. 2009). Similarly, overexpression of Robo4 in the same type of cells led to a suppression of extracellular signal–regulated kinase (ERK) and focal adhesion kinase (FAK) phosphorylation (Seth et al. 2005). Whereas in another study of Robo4 function in the zebrafish vascular system, the authors argued that the activation of Cdc42/Rac1 in ECs is a ligand-dependent function of Robo4 (Kaur et al. 2006). Here, we observed that downregulation of Robo4 caused a marked reduction in the motility of migratory neurons in the absence of any potential ligand, supporting a ligand-independent effect of Robo4 to enhance neuronal motility.

Slit/Robo4 Function in Cortical Development

Neuronal migration is one of the most elaborated processes during brain morphogenesis, which consists of neuronal interaction with extracellular environment and cell-autonomous movement. Several proteins have been identified as essential regulators for the radial migration and lamination of cortical neurons, including transcription factors that specify neuronal subtypes, transmembrane proteins that regulate neuron–glia adhesion, signaling molecules that promote the polarization of newborn neurons, and cytoplasmic components that regulate cytoskeleton dynamics and nuclear translocation (Gleeson and Walsh 2000; Hatten 2002; Ayala et al. 2007; Elias et al. 2007; Vallee et al. 2009). Recently, we discovered that cortical radial migration is guided by gradient of diffusible extracellular factors (Zheng and Yuan 2008). Semaphorin3A, a well-known repulsive axon guidance molecule, may serve as a cortical surface-derived attractive cue to promote the upward radial migration of cortical neurons (Chen, Sima, et al. 2008). Apart from Semaphorins, several other guidance factors are also expressed in a laminar pattern in developing cortex, including the repulsive factors Ephrins and Slits (Metin et al. 2006; Andrews et al. 2007; Torii et al. 2009). It is likely that multiple factors are engaged redundantly in the guidance of neuronal migration to ensure the proper distribution of newborn neurons. Our present experiments revealed a new regulatory role of Robo4 for cortical radial migration partly through desensitizing the newborn neurons to the repulsive signal of CP-derived Slit1. This reminds us of the similar "silencing" mechanism in midline crossing of commissural axons in spinal cord and hindbrain, where Rig-1 (Robo3) functions as a negative regulator of Slit responsiveness by antagonizing the repulsive signal of Robo1/2 (Marillat et al. 2004; Sabatier et al. 2004; Chen, Gore, et al. 2008). However, we did not detect the expression of *robo3* in migrating newborn neurons purified by FACS (Fig. 1*C*). Thus during the radial migration of newborn neurons, it is likely that the repulsion of CP-derived Slit1 is mainly silenced by Robo4 to allow the CP entry of these newborn neurons. On the other hands, Slit protein has been implicated to guide the axon pathfinding of cortical pyramidal neurons and promote their dendritic arborization through Robo1/2 receptors (Dickson and Gilestro 2006; Andrews et al. 2007; Ypsilanti et al. 2010), effects that happen subsequently after the completion of the radial migration of newborn neurons. Thus, the spatiotemporal expression of Robos should be tightly controlled to "switch on and off" the repulsive action of Slits at proper developmental stages. Our finding of Robo4 effect would provide a novel regulation pathway of Slit/Robo signaling during cortical development.

Finally, we note that an SNP of *robo4* gene have been shown to be closely associated with a subpopulation of autism (Anitha et al. 2008), a severe neurodevelopmental disorder defined by social and communication deficits and ritualistic–repetitive behaviors in early childhood (Geschwind 2009; Levy et al. 2009). Some autism patients present the coarse cortical tissues and poor cortical lamination (Amaral et al. 2008). It is of great interest to explore whether *robo4* deficiency is responsible for the brain malformation in this subpopulation of autism patients.

Supplementary Material

Supplementary material can be found at: http://www.cercor.oxfordjournals.org/

Funding

This work was supported by 973 project (2011CBA00400) and the National Natural Science Foundation of China (31021063). X.-Y. Yuan was supported by SA-SIBS Scholarship (2010).

Notes

We thank Dr A. Chedotal for providing the *slit1* riboprobe, Dr J.-G. Geng for providing the human *robo4* cDNA, Dr Q. Hu for technical support in confocal microscopy, J.-Y. Yu for cell culture, Y.-N. Yao for mice genotyping, Y.-T. Yin for IUE experiments, and C.-F. Shang and J. Jiang for data analysis.W.Z. designed the research, conducted most of the *in vivo* and *in vitro* experiments and data analysis and wrote the manuscript; A.-Q.G. prepared most of constructs, carried out the RT-PCR experiments, data analysis, and genotyping of mutant mice; P.-F.L. contributed to mice IUE; Y.W. contributed to mice genotyping and Slit-binding experiments; and X.-B.Y. designed the research, supervised the project, and wrote the manuscript. *Conflict of Interest* : None declared.

References

Amaral DG, Schumann CM, Nordahl CW. 2008. Neuroanatomy of autism. Trends Neurosci. 31:137–145.

Andrews WD, Barber M, Parnavelas JG. 2007. Slit-Robo interactions during cortical development. J Anat. 211:188–198.

Angevine JB Jr, Sidman RL. 1961. Autoradiographic study of cell migration during histogenesis of cerebral cortex in the mouse. Nature. 192:766–768.

Anitha A, Nakamura K, Yamada K, Suda S, Thanseem I, Tsujii M, Iwayama Y, Hattori E, Toyota T, Miyachi T, et al. 2008. Genetic analyses of roundabout (ROBO) axon guidance receptors in autism. Am J Med Genet B Neuropsychiatr Genet. 147B:1019–1027.

Ayala R, Shu T, Tsai LH. 2007. Trekking across the brain: the journey of neuronal migration. Cell. 128:29–43.

Bashaw GJ, Goodman CS. 1999. Chimeric axon guidance receptors: the cytoplasmic domains of slit and netrin receptors specify attraction versus repulsion. Cell. 97:917–926.

Bedell VM, Yeo SY, Park KW, Chung J, Seth P, Shivalingappa V, Zhao J, Obara T, Sukhatme VP, Drummond IA, et al. 2005. roundabout4 is essential for angiogenesis in vivo. Proc Natl Acad Sci U S A. 102:6373–6378.

Berry M, Rogers AW. 1965. The migration of neuroblasts in the developing cerebral cortex. J Anat. 99:691–709.

Bielas S, Higginbotham H, Koizumi H, Tanaka T, Gleeson JG. 2004. Cortical neuronal migration mutants suggest separate but intersecting pathways. Annu Rev Cell Dev Biol. 20:593–618.

Brose K, Bland KS, Wang KH, Arnott D, Henzel W, Goodman CS, Tessier-Lavigne M, Kidd T. 1999. Slit proteins bind Robo receptors and have an evolutionarily conserved role in repulsive axon guidance. Cell. 96:795–806.

Brummelkamp TR, Bernards R, Agami R. 2002. A system for stable expression of short interfering RNAs in mammalian cells. Science. 296:550–553.

Camurri L, Mambetisaeva E, Davies D, Parnavelas J, Sundaresan V, Andrews W. 2005. Evidence for the existence of two Robo3 isoforms with divergent biochemical properties. Mol Cell Neurosci. 30:485–493.

Chen G, Sima J, Jin M, Wang KY, Xue XJ, Zheng W, Ding YQ, Yuan XB. 2008. Semaphorin-3A guides radial migration of cortical neurons during development. Nat Neurosci. 11:36–44.

Chen H, Zhang M, Tang S, London NR, Li DY, Zhang K. 2010. Slit-robo signaling in ocular angiogenesis. Adv Exp Med Biol. 664:457–463.

Chen Z, Gore BB, Long H, Ma L, Tessier-Lavigne M. 2008. Alternative splicing of the Robo3 axon guidance receptor governs the midline switch from attraction to repulsion. Neuron. 58:325–332.

Colon-Ramos DA. 2009. Synapse formation in developing neural circuits. Curr Top Dev Biol. 87:53–79.

Dickson BJ, Gilestro GF. 2006. Regulation of commissural axon pathfinding by slit and its Robo receptors. Annu Rev Cell Dev Biol. 22:651–675.

Elias LA, Wang DD, Kriegstein AR. 2007. Gap junction adhesion is necessary for radial migration in the neocortex. Nature. 448:901–907.

Feldman DE. 2009. Synaptic mechanisms for plasticity in neocortex. Annu Rev Neurosci. 32:33–55.

Fujiwara M, Ghazizadeh M, Kawanami O. 2006. Potential role of the Slit/Robo signal pathway in angiogenesis. Vasc Med. 11:115–121.

Geschwind DH. 2009. Advances in autism. Annu Rev Med. 60:367–380.

Gleeson JG, Walsh CA. 2000. Neuronal migration disorders: from genetic diseases to developmental mechanisms. Trends Neurosci. 23:352–359.

Gressens P. 2005. Neuronal migration disorders. J Child Neurol. 20:969–971.

Guan CB, Xu HT, Jin M, Yuan XB, Poo MM. 2007. Long-range Ca2+ signaling from growth cone to soma mediates reversal of neuronal migration induced by slit-2. Cell. 129:385–395.

Guan KL, Rao Y. 2003. Signalling mechanisms mediating neuronal responses to guidance cues. Nat Rev Neurosci. 4:941–956.

Guerrini R, Filippi T. 2005. Neuronal migration disorders, genetics, and epileptogenesis. J Child Neurol. 20:287–299.

Gupta A, Tsai LH, Wynshaw-Boris A. 2002. Life is a journey: a genetic look at neocortical development. Nat Rev Genet. 3:342–355.

Hashimoto-Torii K, Torii M, Sarkisian MR, Bartley CM, Shen J, Radtke F, Gridley T, Sestan N, Rakic P. 2008. Interaction between Reelin and Notch signaling regulates neuronal migration in the cerebral cortex. Neuron. 60:273–284.

Hatten ME. 1999. Central nervous system neuronal migration. Annu Rev Neurosci. 22:511–539.

Hatten ME. 2002. New directions in neuronal migration. Science. 297:1660–1663.

Hohenester E. 2008. Structural insight into Slit-Robo signalling. Biochem Soc Trans. 36:251–256.

Huminiecki L, Bicknell R. 2000. In silico cloning of novel endothelial-specific genes. Genome Res. 10:1796–1806.

Huminiecki L, Gorn M, Suchting S, Poulsom R, Bicknell R. 2002. Magic roundabout is a new member of the roundabout receptor family that is endothelial specific and expressed at sites of active angiogenesis. Genomics. 79:547–552.

Inoue T, Krumlauf R. 2001. An impulse to the brain—using in vivo electroporation. Nat Neurosci. 4:1156–1158.

Jones CA, London NR, Chen H, Park KW, Sauvaget D, Stockton RA, Wythe JD, Suh W, Larrieu-Lahargue F, Mukouyama YS, et al. 2008. Robo4 stabilizes the vascular network by inhibiting pathologic angiogenesis and endothelial hyperpermeability. Nat Med. 14:448–453.

Jones CA, Nishiya N, London NR, Zhu W, Sorensen LK, Chan AC, Lim CJ, Chen H, Zhang Q, Schultz PG, et al. 2009. Slit2-Robo4 signalling promotes vascular stability by blocking Arf6 activity. Nat Cell Biol. 11:1325–1331.

Kapfhammer JP, Xu H, Raper JA. 2007. The detection and quantification of growth cone collapsing activities. Nat Protoc. 2:2005–2011.

Kaur S, Castellone MD, Bedell VM, Konar M, Gutkind JS, Ramchandran R. 2006. Robo4 signaling in endothelial cells implies attraction guidance mechanisms. J Biol Chem. 281:11347–11356.

Kaur S, Samant GV, Pramanik K, Loscombe PW, Pendrak ML, Roberts DD, Ramchandran R. 2008. Silencing of directional migration in roundabout4 knockdown endothelial cells. BMC Cell Biol. 9:61.

Kidd T, Bland KS, Goodman CS. 1999. Slit is the midline repellent for the robo receptor in Drosophila. Cell. 96:785–794.

Koch AW, Mathivet T, Larrivee B, Tong RK, Kowalski J, Pibouin-Fragner L, Bouvree K, Stawicki S, Nicholes K, Rathore N, et al. 2011. Robo4 maintains vessel integrity and inhibits angiogenesis by interacting with UNC5B. Dev Cell. 20:33–46.

Legg JA, Herbert JM, Clissold P, Bicknell R. 2008. Slits and Roundabouts in cancer, tumour angiogenesis and endothelial cell migration. Angiogenesis. 11:13–21.

Levy SE, Mandell DS, Schultz RT. 2009. Autism. Lancet. 374:1627–1638.

Li HS, Chen JH, Wu W, Fagaly T, Zhou L, Yuan W, Dupuis S, Jiang ZH, Nash W, Gick C, et al. 1999. Vertebrate slit, a secreted ligand for the transmembrane protein roundabout, is a repellent for olfactory bulb axons. Cell. 96:807–818.

Liao WX, Wing DA, Geng JG, Chen DB. 2010. Perspectives of SLIT/ROBO signaling in placental angiogenesis. Histol Histopathol. 25:1181–1190.

London NR, Zhu W, Bozza FA, Smith MC, Greif DM, Sorensen LK, Chen L, Kaminoh Y, Chan AC, Passi SF, et al. 2010. Targeting Robo4-dependent Slit signaling to survive the cytokine storm in sepsis and influenza. Sci Transl Med. 2:23ra19.

LoTurco JJ, Bai JL. 2006. The multipolar stage in neuronal migration. Trends Neurosci. 29:407–413.

Mambetisaeva ET, Andrews W, Camurri L, Annan A, Sundaresan V. 2005. Robo family of proteins exhibit differential expression in mouse spinal cord and Robo-Slit interaction is required for midline crossing in vertebrate spinal cord. Dev Dyn. 233:41–51.

Marillat V, Cases O, Nguyen-Ba-Charvet KT, Tessier-Lavigne M, Sotelo C, Chedotal A. 2002. Spatiotemporal expression patterns of slit and robo genes in the rat brain. J Comp Neurol. 442:130–155.

Marillat V, Sabatier C, Failli V, Matsunaga E, Sotelo C, Tessier-Lavigne M, Chedotal A. 2004. The slit receptor Rig-1/Robo3 controls midline crossing by hindbrain precerebellar neurons and axons. Neuron. 43:69–79.

Marin O, Rubenstein JL. 2003. Cell migration in the forebrain. Annu Rev Neurosci. 26:441–483.

Marin O, Valiente M, Ge X, Tsai LH. 2010. Guiding neuronal cell migrations. Cold Spring Harb Perspect Biol. 2:a001834.

Marlow R, Binnewies M, Sorensen LK, Monica SD, Strickland P, Forsberg EC, Li DY, Hinck L. 2010. Vascular Robo4 restricts proangiogenic VEGF signaling in breast. Proc Natl Acad Sci U S A. 107:10520–10525.

Marteau L, Pacary E, Valable S, Bernaudin M, Guillemot F, Petit E. 2011. Angiopoietin-2 regulates cortical neurogenesis in the developing telencephalon. Cereb Cortex. 21:1695–1702.

McManus MF, Golden JA. 2005. Neuronal migration in developmental disorders. J Child Neurol. 20:280–286.

Metin C, Baudoin JP, Rakic S, Parnavelas JG. 2006. Cell and molecular mechanisms involved in the migration of cortical interneurons. Eur J Neurosci. 23:894–900.

Morlot C, Thielens NM, Ravelli RB, Hemrika W, Romijn RA, Gros P, Cusack S, McCarthy AA. 2007. Structural insights into the Slit-Robo complex. Proc Natl Acad Sci U S A. 104:14923–14928.

Nguyen Ba-Charvet KT, Brose K, Marillat V, Kidd T, Goodman CS, Tessier-Lavigne M, Sotelo C, Chedotal A. 1999. Slit2-mediated chemorepulsion and collapse of developing forebrain axons. Neuron. 22:463–473.

O'Donnell M, Chance RK, Bashaw GJ. 2009. Axon growth and guidance: receptor regulation and signal transduction. Annu Rev Neurosci. 32:383–412.

Park KW, Morrison CM, Sorensen LK, Jones CA, Rao Y, Chien CB, Wu JY, Urness LD, Li DY. 2003. Robo4 is a vascular-specific receptor that inhibits endothelial migration. Dev Biol. 261:251–267.

Rakic P. 1972. Mode of cell migration to the superficial layers of fetal monkey neocortex. J Comp Neurol. 145:61–83.

Rakic P. 1990. Principles of neural cell migration. Experientia. 46:882–891.

Rakic P, Lombroso PJ. 1998. Development of the cerebral cortex: I. Forming the cortical structure. J Am Acad Child Adolesc Psychiatry. 37:116–117.

Reynolds A, Leake D, Boese Q, Scaringe S, Marshall WS, Khvorova A. 2004. Rational siRNA design for RNA interference. Nat Biotechnol. 22:326–330.

Sabatier C, Plump AS, Le M, Brose K, Tamada A, Murakami F, Lee EY, Tessier-Lavigne M. 2004. The divergent Robo family protein rig-1/Robo3 is a negative regulator of slit responsiveness required for midline crossing by commissural axons. Cell. 117:157–169.

Saito T, Nakatsuji N. 2001. Efficient gene transfer into the embryonic mouse brain using in vivo electroporation. Dev Biol. 240:237–246.

Sanada K, Tsai LH. 2005. G protein betagamma subunits and AGS3 control spindle orientation and asymmetric cell fate of cerebral cortical progenitors. Cell. 122:119–131.

Seth P, Lin Y, Hanai J, Shivalingappa V, Duyao MP, Sukhatme VP. 2005. Magic roundabout, a tumor endothelial marker: expression and signaling. Biochem Biophys Res Commun. 332:533–541.

Sheldon H, Andre M, Legg JA, Heal P, Herbert JM, Sainson R, Sharma AS, Kitajewski JK, Heath VL, Bicknell R. 2009. Active involvement of Robo1 and Robo4 in filopodia formation and endothelial cell motility mediated via WASP and other actin nucleation-promoting factors. FASEB J. 23:513–522.

Song H, Poo M. 2001. The cell biology of neuronal navigation. Nat Cell Biol. 3:E81–E88.

Suchting S, Heal P, Tahtis K, Stewart LM, Bicknell R. 2005. Soluble Robo4 receptor inhibits in vivo angiogenesis and endothelial cell migration. FASEB J. 19:121–123.

Torii M, Hashimoto-Torii K, Levitt P, Rakic P. 2009. Integration of neuronal clones in the radial cortical columns by EphA and ephrin-A signalling. Nature. 461:524–528.

Vallee RB, Seale GE, Tsai JW. 2009. Emerging roles for myosin II and cytoplasmic dynein in migrating neurons and growth cones. Trends Cell Biol. 19:347–355.

Verissimo AR, Herbert JM, Heath VL, Legg JA, Sheldon H, Andre M, Swain RK, Bicknell R. 2009. Functionally defining the endothelial transcriptome, from Robo4 to ECSCR. Biochem Soc Trans. 37:1214–1217.

Weitzman M, Bayley EB, Naik UP. 2008. Robo4: a guidance receptor that regulates angiogenesis. Cell Adh Migr. 2:220–222.

Whitford KL, Marillat V, Stein E, Goodman CS, Tessier-Lavigne M, Chedotal A, Ghosh A. 2002. Regulation of cortical dendrite development by Slit-Robo interactions. Neuron. 33:47–61.

Xue XJ, Yuan XB. 2010. Nestin is essential for mitogen-stimulated proliferation of neural progenitor cells. Mol Cell Neurosci. 45:26–36.

Ypsilanti AR, Zagar Y, Chedotal A. 2010. Moving away from the midline: new developments for Slit and Robo. Development. 137:1939–1952.

Yu TW, Bargmann CI. 2001. Dynamic regulation of axon guidance. Nat Neurosci. 4:1169–1176.

Zhao CT, Li K, Li JT, Zheng W, Liang XJ, Geng AQ, Li N, Yuan XB. 2009. PKCdelta regulates cortical radial migration by stabilizing the Cdk5 activator p35. Proc Natl Acad Sci U S A. 106:21353–21358.

Zheng W, Yuan X. 2008. Guidance of cortical radial migration by gradient of diffusible factors. Cell Adh Migr. 2:48–50.